applied sciences

MDPI

Article

Hygroscopicity and Morphology of Bio-Based Boards—The Influence of the Formulation

Eleonora Cintura [1,2,*], Lina Nunes [2,3], Luisa Molari [4], Matteo Bettuzzi [5], Maria Pia Morigi [5], Rosa Brancaccio [5] and Paulina Faria [1,*]

1 Civil Engineering Research and Innovation for Sustainability (CERIS), Department of Civil Engineering, NOVA School of Science and Technology, NOVA University Lisbon, Caparica, 2829-516 Almada, Portugal
2 Structures Department, National Laboratory for Civil Engineering, 1700-066 Lisbon, Portugal; linanunes@lnec.pt
3 Centre for Ecology, Evolution and Environmental Changes (CE3C), Global Change and Sustainability Institute, University of the Azores, 9700-042 Angra do Heroísmo, Portugal
4 Department of Civil, Chemical, Environmental and Materials Engineering (DICAM), Alma Mater Studiorum-University of Bologna, 40136 Bologna, Italy; luisa.molari@unibo.it
5 Department of Physics and Astronomy "Augusto Righi" (DIFA), Alma Mater Studiorum-University of Bologna, 40127 Bologna, Italy; matteo.bettuzzi@unibo.it (M.B.); mariapia.morigi@unibo.it (M.P.M.); rosa.brancaccio@unibo.it (R.B.)
* Correspondence: e.cintura@fct.unl.pt (E.C.); paulina.faria@fct.unl.pt (P.F.)

Abstract: The internal structures and the hygroscopicity of bio-based boards consisting of giant reed (*Arundo donax* L.) and hazelnut shells as bio-aggregates, and a sodium silicate solution as the adhesive, were investigated. The aim was to evaluate the influence of each material (the bio-aggregates and adhesive) and their distributions in the boards on the final performance. By carrying out X-ray computed tomography, the internal structures and the porosities of the boards were determined, allowing important considerations of their hygroscopicity. The voids' percentages were between 26% and 36% of the total volume of the composites. Both the materials and the composites demonstrated high hygroscopicity. In particular, the mixtures of the bio-aggregates and the sodium silicate allowed reaching a moisture buffering value of 7.44 g/(m^2%RH) for the *A. donax*-based composite, 3.86 g/(m^2%RH) for the hazelnut-shell-based composite, and 4.65 g/(m^2%RH) for the mixture-based composite. Besides the identification of the contributions of the materials, a detailed discussion of the assessed properties was carried out to use these bio-based boards in vernacular historic construction. The results show how the aggregate type and the adhesive content affected the final behavior, demonstrating the importance of a conscious material choice. Furthermore, helpful information for the future development of these types of bio-based boards and their possible optimization was provided.

Keywords: agro-industrial waste; *Arundo donax*; bio-aggregate; bio-resource; giant reed; hazelnut shell; hygroscopicity; moisture buffering; sodium silicate; tomography

Citation: Cintura, E.; Nunes, L.; Molari, L.; Bettuzzi, M.; Morigi, M.P.; Brancaccio, R.; Faria, P. Hygroscopicity and Morphology of Bio-Based Boards—The Influence of the Formulation. *Appl. Sci.* **2024**, *14*, 873. https://doi.org/10.3390/app14020873

Academic Editor: Yuebing Sun

Received: 11 December 2023
Revised: 5 January 2024
Accepted: 17 January 2024
Published: 19 January 2024

1. Introduction

Research is nowadays increasingly focused on studying and proposing innovative and sustainable solutions practices. The environmental impact of the construction sector (for new construction, refurbishment, use, and deconstruction) is widely recognized [1,2], as well as the worldwide interest in reducing the production of toxic and environmentally damaging substances [3]. Both the Agenda 2023 [4] and the European Green Deal [1], among several proposals, have reported the need for a reduction in energy demand and the encouragement of a circular economic system. Thus, among the investigated innovative possibilities, the use of bio-wastes and bio-resources seems to be a particularly attractive solution. It reduces energy consumption [5], ensures a circular economy, and moderates the problem of waste disposal [6,7]. Furthermore, the use of these types of materials, which

do not act as water vapor barriers, can guarantee cultural heritage preservation, namely, vernacular architecture.

Past research has already considered bio-based building composites and assessed their properties. Both bio-wastes (such as agro-industrial wastes) and bio-resources have been investigated (such as straw [8], corn pith [9], rice husk [10], banana fibers [11], hemp shives [12], and reed [13]). Depending on the biomaterials used, the bio-based composites demonstrated different promising properties, namely, good thermal insulation performance, sound absorption capacity, high hygroscopicity, or adequate mechanical resistance. Several types of bio-based composites and products have been produced and studied, such as plastering mortars [14], glues [15], bricks [16], and boards [17,18], which are the ones considered in this study.

Bio-based boards are usually made of bio-aggregates (bio-wastes or bio-resources) and an adhesive (glue or binder). In addition to the bio-wastes/bio-resources, the employed adhesive also significantly influences the board's final properties, as well as its sustainability and toxicity [19,20]. Considering the same bio-aggregates and different adhesives, the composites' behaviors deeply change [21]. Using adhesives that could be harmful to human health, such as formaldehyde-based ones [22,23], reduces the non-toxicity and the eco-efficiency derived from the use of bio-based materials. The selected adhesive could also moderate some of the main drawbacks, such as low resistance to water, fire, and biological attack [24–26], improving the final composite's performance. Thus, knowing the properties of both the aggregates and the adhesive, individually and in composites, is crucial in building composites' production [27,28].

The present work addresses the topic of materials' influence on the final performance of composite boards. In particular, this research study considered bio-based boards made of bio-aggregates, namely, hazelnut shells and giant reed (*Arundo donax* L.), bounded by a sodium silicate solution [29,30] (these two reference studies provided characterizations of the proposed composites, evaluating their physical and mechanical properties).

Hazelnut shells are a widely produced bio-waste [29], available throughout the year due to hazelnut treatment before their use [31]. Some past studies have already considered the possibility of using hazelnut shells for building practices [32,33]. Nevertheless, they have not been largely investigated as such [34]. *A. donax* L., known as giant reed or giant cane, is an herbaceous, perennial, non-food, invasive, and largely available bio-resource [35]. It can be found worldwide due to its tolerance to different climates and soil conditions [5]. It has already been employed for construction practices—i.e., in panels, concrete, plasters, and new construction technologies—showing promising mechanical and thermal properties [13]. Being natural products, both bio-aggregates could be employed in innovative building products compatible with vernacular architectural elements [36,37]. Indeed, they would be compatible with the traditional walls and roofs and could ensure their preservation.

Sodium silicate, also known as "water glass", is a widely produced material, which has demonstrated several benefits. It is water-soluble, fire-resistant, non-toxic, and, hence, not dangerous to human health, environment-friendly, and economically convenient [38–40]. It has been employed in several sectors, such as to produce detergents and cleaning compounds [38], for material treatments [40], in ceramics [41], and in the production of geopolymers [42] and concretes [43]. Among its several uses, the employment of sodium silicate as a binder to produce bio-based building composites could be a promising possibility [44]. Indeed, in addition to guaranteeing the feasibility of their production, it can reduce some of the main weaknesses derived from their organic matrices, improving their resistance to fire [45] and preventing chemical decomposition [46,47]. Some past studies have investigated the employment of sodium silicate as an adhesive for bio-based building boards. For example, Bakatovich et al. [39] evaluated the properties of reed and straw fiber-based composites bonded with sodium silicate and rosin, and Liuzzi et al. [46] produced composites made of olive fibers and straw and a sodium silicate solution as the adhesive. Both studies reported promising thermal insulation performance of the composites. Cintura et al. [21] considered some bio-based

boards bounded with different adhesives and evaluated their biological susceptibility without inoculation. The composites with sodium silicate demonstrated the highest resistance, avoiding mold growth at high relative humidity levels. Besides its several benefits, it has also shown some drawbacks, such as high hygroscopicity and low moisture resistance [45,48], which could cause the degradation of the materials [49]. Furthermore, it could be less eco-efficient than other adhesives (i.e., bio-based ones or natural glues). Indeed, higher temperatures could be required for its production [38], even if lower than those required for other widely used adhesives (such as cement-based binders).

As hazelnut-shell-based and *A. donax*-based boards have demonstrated interesting hygroscopic behavior [29,30], which can be useful to passively contribute to indoor comfort [50], reducing energy consumption [51], the present study mainly considered this property. The contribution of each material was investigated by testing them individually and in composites. Furthermore, the materials' dispositions in the proposed boards were analyzed, assessing the correlation between the hygroscopicity and internal structure. X-ray computed tomography, which is a non-invasive 3D-imaging technique able to supply crucial information on the studied products [52], ensured the evaluation of the internal configurations of the boards. This technique has been employed in several fields, such as medical, industrial, and cultural heritage [53], as well as to investigate bio-based composites [54]. It provides information such as the pore size distribution, porosity, and tortuosity of the porous network [55]. In this work, X-ray computed tomography ensured the identification of the distributions of the aggregates and adhesive and the porosities of the bio-based boards. Finally, statistical analysis (ANOVA) was carried out for further consideration of the results.

The present work aimed to analyze the composites' properties and define the influence of each material on the final performance, both in terms of the materials' properties and the aggregate/adhesive's internal distribution.

2. Materials and Specimens

2.1. Bio-Aggregates and Adhesive

Giant reed (*Arundo donax* L.) and hazelnut shells were selected as bio-aggregates, characterized, and prepared as described in past studies [29–31]. *A. donax* was harvested from the cultivation of the Department of Agricultural and Food Sciences, the University of Bologna, in Ozzano dell'Emilia, Bologna, Italy. Hazelnut shells were provided by Raccolti di Cin, Baldissero d'Alba, Cuneo, Italy. Both were shredded to have grain sizes mainly between 4 mm and 8 mm and dried at T = 60 °C until reaching a constant mass (with a variation in mass of ≤0.1% after 24 h) [29,30].

Figure 1, adapted from the reference studies in [29–31], shows the particle size distributions of both bio-aggregates.

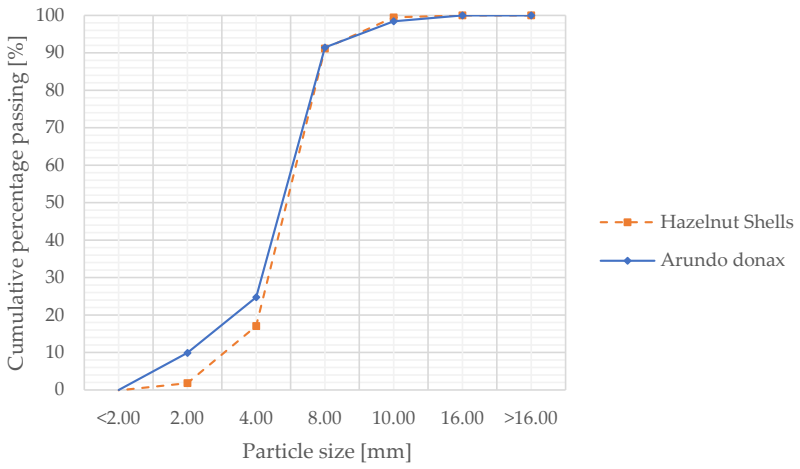

Figure 1. Particle size distributions of Arundo donax and hazelnut shells.

A sodium silicate solution, $Na_2O{\cdot}n(SiO_2)$, provided by Ingessil Srl, Montorio, Verona, Italy, with a density of 1.471 g/mL, a sodium silicate concentration of 41.33% p/p, and pH (T = 20 °C) of 12.40, was employed as the adhesive, coherent with the reference studies [29,30].

2.2. Composite Samples Preparation

The samples were produced as described by Cintura et al. [29,30]. The same percentages of the bio-aggregates/adhesive and the same production process were considered. They were selected after several tests, maximizing the contents of the aggregates, minimizing the amount of the adhesive, and securing sufficient mechanical resistance. The selected percentages were 70% aggregates and 30% adhesive (by total volume).

Table 1 shows the mix designs and the composites' designations. As for the latter, the first letters of the materials were considered (**A** = ***A****. donax*, **H** = **h**azelnut shells, and **AH** = ***A****. donax* + **h**azelnut shells).

Table 1. Mix designs (quantities of aggregates and adhesives in percentages by the total volume) and the composites' designations considered for the experimental analysis.

Composite's Designation	Materials' Quantities (% by Total Volume)		
	A. donax	**Hazelnut Shells**	**Sodium Silicate Solution**
A	70	-	30
H	-	70	30
AH	35	35	30

The bio-aggregates and the sodium silicate solution were mechanically mixed for 10 min, placed into silicon molds without compaction, and leveled using a spatula to obtain a horizontal surface. The molds were closed and maintained at T = 60 °C for 3 h and then under laboratory conditions (air-dried), always being rotated to secure a homogeneous distribution of the sodium silicate solution [31]. After 2 days, the samples were de-molded and cured under laboratory conditions for 28 days. To secure complete drying, they were finally dried at T = 50 °C until reaching a constant mass (a variation in mass of less than 0.5% after 24 h) [46,56]. The composite samples were analyzed after being dried under this condition.

Cylindrical (diameter = 10 cm; thickness = 4 cm) and rectangular (10 cm × 10 cm; thickness = 4 cm) samples were produced to be employed for different analyses (as described in the following section). Figure 2 shows the produced samples. Three replications for each composite were considered.

As better detailed in the following section, the materials (bio-aggregates and adhesive, individually) were tested too. In this case, the bio-aggregates were employed after the preparation described in Section 2.1 (i.e., after shredding and drying at T = 60 °C until reaching a constant mass). For the designations, the repetition of the letters was considered: ***A****. donax* = **AA**; **h**azelnut shells = **HH**; and ***A****. donax* + **h**azelnut shells = **AAHH**. Again, three samples for each bio-aggregate were tested. As for the adhesive, the sodium silicate solution was placed in a rectangular silicon mold (10 cm × 10 cm) and left to air-dry under laboratory conditions for 28 days. The employed designation was **S** (= **s**odium silicate solution), and four replications were considered.

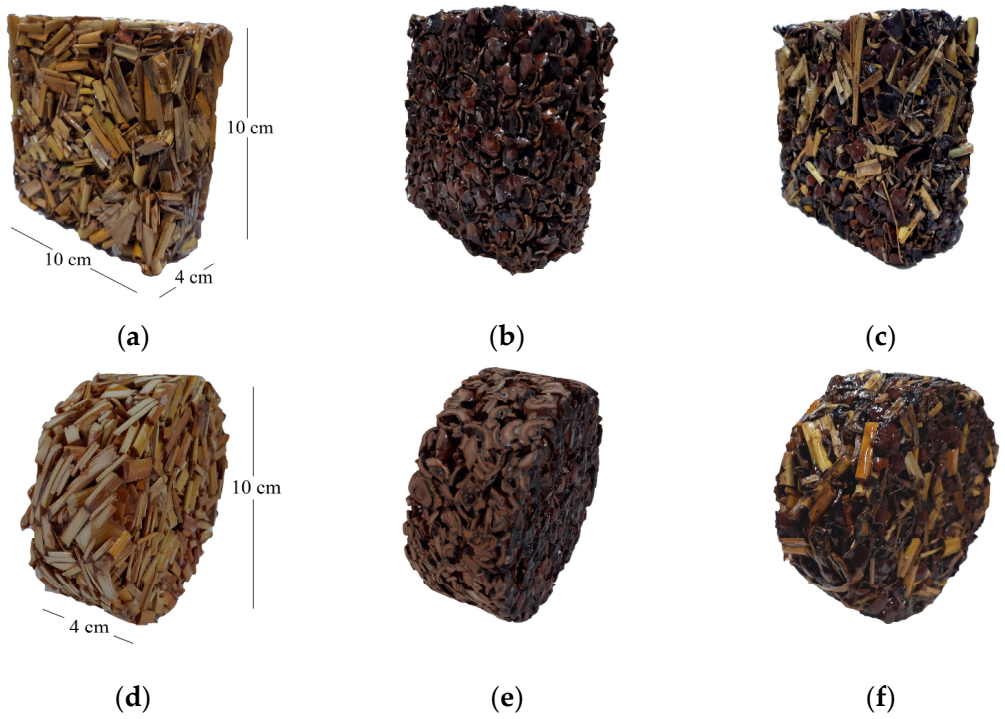

Figure 2. Composite samples made of bio-aggregates and sodium silicate solution. Rectangular and cylindrical samples: (**a**,**d**) *A. donax*-based composite—A; (**b**,**e**) hazelnut-shell-based composite—H; and (**c**,**f**) *A. donax* + hazelnut-shell-based composite—AH.

3. Test Methods

Table 2 summarizes the tests performed, the numbers, sizes, and designations of the samples used, and the considered references.

Table 2. Tests performed, numbers, sizes, and designations of the samples, and references.

Property	Material	Samples			Ref.
		N.	Size (cm)	Designations	
Apparent density	*A. donax*	3	10 × 10, h = 4	A1, A2, and A3	Adaptation of EN 323 [57]
	Hazelnut shells	3	10 × 10, h = 4	H1, H2, and H3	
	Mixture	3	10 × 10, h = 4	AH1, AH2, and AH3	
Tomography	*A. donax*	3	d = 10, h = 4	A4, A5, and A6	-
	Hazelnut shells	3	d = 10, h = 4	H4, H5, and H6	
	Mixture	3	d = 10, h = 4	AH4, AH5, and AH6	
Hygroscopicity of materials	*A. donax*	3	15 × 11, h = 2	AA1, AA2, and AA3	Adaptation of ISO 24353 [58]
	Hazelnut shells	3	15 × 11, h = 2	HH1, HH2, and HH3	
	Mixture *	3	15 × 11, h = 2	AAHH1, AAHH2, and AAHH3	
	Sodium silicate	4	10 × 10 × h *	S1, S2, S3, and S4	
Hygroscopicity of composites	*A. donax*	3	10 × 10 × 4	A1, A2, and A3	ISO 24353 [58]
	Hazelnut shells	3	10 × 10 × 4	H1, H2, and H3	
	Mixture	3	10 × 10 × 4	AH1, AH2, and AH3	

* Note: Mixture = 50% *A. donax*–50% hazelnut shells of the total volume of the filled container (without adhesive); sodium silicate = samples of the air-dried (lab. conditions) sodium silicate solution with a thickness (h) varying between 2 and 4 mm.

3.1. Apparent Density

An adaptation of EN 323 [57] was considered to determine the apparent density of the composites. Three prismatic samples of each composition (A1, A2, and A3; H1, H2, and H3; and AH1, AH2, and AH3) of 10 cm × 10 cm × 4 cm (Figure 2a–c) were stabilized at

T = 50 °C (with a variation in mass of less than 0.5% after 24 h), weighed with a Kern EW 2200-2NM electronic balance, and measured with a Fervi digital caliper. The ratios between the mass and volume were calculated, and the average values and the standard deviations were determined.

3.2. Internal Structure and Porosity

Three cylindrical samples of each composition (A4, A5, A6, H4, H5, H6, AH4, AH5, and AH6), with diameter = 10 cm and h = 4 cm (Figure 2d–f), were used to analyze their internal structures and porosities using X-ray computed tomography. For this purpose, a CT system was used. The apparatus (Figure 3a) was assembled in-house (byPhysics and Astronomy Department of the University of Bologna) as a multipurpose CT system and consisted of a Bosello XRG120.IT conventional X-ray tube, a Varian PaxScan 2520D flat-panel X-ray detector, and a Physik Instrument manipulation axis set with an M-038 micrometric sample rotation stage and M413.3PD for detector translation. The samples were placed with one face over the rotation stage in a horizontal position.

(**a**) (**b**)

Figure 3. X-ray computed tomography: (**a**) employed apparatus; (**b**) three samples separated with expanded polystyrene boards placed on the rotation platform.

Two or three samples, separated with expanded polystyrene boards (which are transparent to X-rays), were placed vertically on the rotation platform, one on top of the other (Figure 3b), to optimize the scanning time. A standard scanning protocol for the system was used: 900 projections over a 360-degree angle; a 4-frame average for each projection; and low magnification (M = 1.115). The voltage (70 kV), current (6.5 mA), and detector frame rate (3 fps) were chosen according to the sample size and material after an initial evaluation of the X-ray absorption and signal outcome in the detector. No filtration was used. The overall scanning time was 1 h.

After scanning each group of samples, CT slices were obtained via raw data elaborations with the in-house software PARREC, EXE_2023_01_26_ PARREC_BHC_AV, (implementing a standard version of the filtered back-projections cone-beam Feldkamp algorithm [59]). One of the great strengths of the performed X-ray computed tomography was the large number of reconstructed slices, which ensured the reproduction of the entire internal structures of the samples at a high resolution.

Slices produced with the reconstruction software were imported into the ImageJ/Fiji 1.53c freeware image processing software for a more convenient data visualization and further elaboration via a segmentation and pore classification process (Section 4.2). The three-dimensional rendering of the reconstructed X-ray-scanned objects and the first simple overall porosity measurements were performed by importing CT slices with the VGStudioMax 2.1 commercial software (Volume Graphics).

It is important to underline that although the samples employed for the tomography were not the same as those employed for the hygroscopic analysis (described in the following Section 3.3), the results were considered significant to carry out a comparison between the internal structures and hygroscopicity as all the samples were produced at the same time with the same mixtures of the aggregate–adhesive, production process, and conditions.

3.3. Hygroscopic Properties

The hygroscopicity (i.e., the ability to adsorb/release moisture under relative humidity (RH) variations [60]) can be determined via several tests, divided into those performed using the step response method and those performed in a flux chamber [61]. In the present study, the step response method was considered, according to ISO 24353 [58]. The variation in mass over time was evaluated for both the materials (the bio-aggregates and adhesive, considered separately: AA, HH, AAHH, and S) and the composites (A, H, and AH).

The bio-aggregates were placed in plastic boxes with open-top surfaces and filled up to a height of 2 cm (Figure 4a), as described by Cintura et al. [28]. This ensured the exposure of only one sample face (15 cm × 11 cm). Three replicates of each bio-aggregate were tested (AA1, AA2, and AA3; HH1, HH2, and HH3) as well as the mixture of 50% *A. donax* and 50% hazelnut shells (AAHH1, AAHH2, and AAHH3).

(**a**) (**b**) (**c**) (**d**)

Figure 4. Samples for the hygroscopicity test: (**a**) plastic boxes (15 cm × 11 cm) filled up to 2 cm with the different aggregates (samples AA, HH, and AAHH); (**b**) air-dried sodium silicate solution covered with aluminum foil, except for the exposure surface (area = 0.1 m^2); (**c**) composite samples (aggregates + sodium silicate solution) A, H, and AH (10 cm × 10 cm × 4 cm) covered with aluminum foil, except for the exposure surface (area = 0.1 m^2); and (**d**) samples in the climatic chamber.

As for the dried sodium silicate solution and the composites, a moisture barrier was provided using aluminum foil (Figure 4b,c), according to ISO 24353 [58] and the method described by Cintura et al. [29,30]. Thus, only the top surface (area = 0.1 m^2) was exposed. Four replicates of the dried sodium silicate solution of 10 cm × 10 cm and a thickness between 2 and 4 mm (S1, S2, S3, and S4) were tested (Figure 4b). As for the composites, three samples of 10 cm × 10 cm and a thickness of 4 cm for each composite—the same employed to evaluate the apparent density—were considered (Figure 4c).

The samples were exposed to four cycles of 24 h (a 12 h sorption phase at 75% RH and a 12 h desorption phase at 50% RH) using a climatic chamber (Climatest ARGOLab CH 250) after being pre-conditioned at T = 23 °C and RH = 63% (Figure 4d) until reaching a constant mass (with a change in mass not higher than 0.5% over 24 h). The samples were weighed every 3 h to determine the moisture adsorption ($\rho_{A,ac}$) and desorption content ($\rho_{A,dc}$), moisture content difference ($\rho_{A,sc}$), and, thus, the sorption/desorption capacity, as indicated in ISO 24353 [58] and described in Equations (1)–(3).

$$\rho_{A,ac}\left[\frac{kg}{m^2}\right] = \frac{m_{an} - m_{d(n-1)}}{Area} \quad (1)$$

$$\rho_{A,dc}\left[\frac{kg}{m^2}\right] = \frac{m_{an} - m_{dn}}{Area} \quad (2)$$

$$\rho_{A,sc}\left[\frac{kg}{m^2}\right] = \rho_{A,ac} - \rho_{A,dc} \quad (3)$$

where m_{an} (kg) is the mass at the end of the sorption phase of the considered cycle, $m_{d(n-1)}$ (kg) is the mass at the end of the previous desorption cycle, m_{dn} (kg) is the mass at the end of the desorption phase of the considered cycle, and Area (m^2) is the exposed surface.

The moisture buffering value (MBV) quantifies the content of adsorbed and released moisture considering cycling between two levels of RH [62,63]. It was calculated considering the average value between the MBV of the sorption, MBV_a (Equation (4)), and the desorption phase, MBV_d (Equation (5)), of the last three cycles [29,30].

$$MBV_a\left[\frac{g}{m^2\%RH}\right] = \frac{m_{an} - m_{d(n-1)}}{\text{Area x}\left(RH_{high} - RH_{low}\right)} \quad (4)$$

$$MBV_d\left[\frac{g}{m^2\%RH}\right] = \frac{m_{an} - m_{dn}}{\text{Area x}\left(RH_{high} - RH_{low}\right)} \quad (5)$$

where the RH_{high} and RH_{low} are 75% and 50%, respectively [58]. The samples were classified by adapting the method described by Rode et al. [64], and the results were compared with values in past studies and literature. It is important to underline that the classification was provided considering the study by Rode et al. [64], although the evaluation was carried out considering the ISO 24353 [58], as the considered method could determine differences in the results [61,65].

3.4. Statistical Analysis

An analysis of variance (ANOVA) was performed using MATLAB R2023a to define if the materials (considered as the variable) identified statistically distinguishable groups, both individually and in composites. Although three samples for each group were tested, this screening test provided an idea of the influences of the employed bio-aggregates in the final performance.

Analysis of variance (ANOVA) tests if the null hypothesis (H0)—which considers the analyzed groups as equal—is verified. Hence, if the H0 is true, the groups are not distinguishable; otherwise, the alternative hypothesis is confirmed, and at least one of the means is different. Once the groups are defined, the experimental data are analyzed with descriptive statistical values, namely, the *p*-value and F-value [66,67]. If the F-value is higher than 1 and the *p*-value is higher than 0.05, the null hypothesis (H0) is confirmed (there are no distinguishable groups). If the F-value is less than 1 and the *p*-value is less than 0.05, the H0 is, hence, false, and the alternative hypothesis is confirmed.

The considered groups were the three composites (the *A. donax*-based one (A), hazelnut-shell-based one (H), and mixture-based one (AH)) regarding their apparent densities and porosities. For the hygroscopicity, the three bio-aggregates (*A. donax* (AA), hazelnut shells (HH), and the mixture of *A. donax* and hazelnut shells (AAHH)) were considered, too. The selected significance level was 5%, and the *p*-values were analyzed to determine if the null hypothesis (H0 = no differences between the groups) was verified. Post hoc tests were performed using a multiple-comparison test.

4. Results and Discussion

4.1. Apparent Density

Table 3 reports the results of the apparent densities of the three samples for each composite, the average values, and standard deviations (SD).

The values of the apparent density were in line with the ones in past studies that considered *A. donax*-based and hazelnut-shell-based composites, namely, 517 kg/m^3 and 702 kg/m^3, respectively [29,30].

The distribution of the aggregates and the sodium silicate was not controlled during the production process. Hence, the samples could have had some differences in aggregate

sizes, internal porosity, and void volume. The variations between the samples of the same composite may have determined some differences in the results of other properties (e.g., the hygroscopicity, as discussed in the following section). However, as the standard deviation related to the average value was low, good uniformity between the tested samples was guaranteed. Moreover, it seemed that better homogeneity was ensured for the hazelnut-shell-based composite.

Table 3. Results of apparent densities at T = 50 °C and porosities: individual and average values and standard deviation (SD).

Composite Samples	Apparent Density (kg/m^3)	Voids (%) *	Solids (%) *
A. donax			
A1	416	-	-
A2	438	-	-
A3	555	-	-
A4	-	26	74
A5	-	35	65
A6	-	33	67
Average value ± SD	470 ± 75	31 ± 5	69 ± 5
Hazelnut shells			
H1	628	-	-
H2	723	-	-
H3	680	-	-
H4	-	35	65
H5	-	38	62
H6	-	34	66
Average value ± SD	677 ± 47	36 ± 2	64 ± 2
A. donax + hazelnut shells			
AH1	667	-	-
AH2	576	-	-
AH3	579	-	-
AH4	-	21	79
AH5	-	27	73
AH6	-	29	71
Average value ± SD	607 ± 52	26 ± 4	74 ± 4

* Note: Percentages by total volume.

The *A. donax*-based composite showed the lowest values of apparent density, followed by the mixture of the two aggregates. The hazelnut-shell-based composite had the highest values. Thus, *A. donax* lowered the apparent density in the mixture-based composite. These results are coherent with the expectation, and there was some correspondence with the values of the loose bulk density of the two aggregates. For the hazelnut shells, the loose bulk density was higher than that for *A. donax*—469 kg/m^3 and 181.3 kg/m^3, respectively [29,30].

4.2. Internal Structure and Porosity

Figure 5 reports one sample for each composite and its internal structures, showing both transverse and longitudinal sections, acquired from ImageJ/Fiji software. For a more precise comparison, the same sections were considered for each sample. Among all the frames, the middle one (i.e., ½ of the total number of frames) and the quarter ones (¼ and ¾ of the total number of frames) were reported. This allowed showing the successive sections of the internal structure, simplifying it.

These results provide a visual evaluation of the homogeneity of the samples and the internal configurations of the aggregate–adhesive combinations. Indeed, Figure 5 shows the sizes and shapes of the voids, the possible connections between the internal voids, the orientations of the aggregates, and the distributions of the sodium silicate solution. In both the transverse and longitudinal sections, the white parts represent the sodium silicate; the grey parts represent the aggregates; and the black parts (inside the samples) represent the voids.

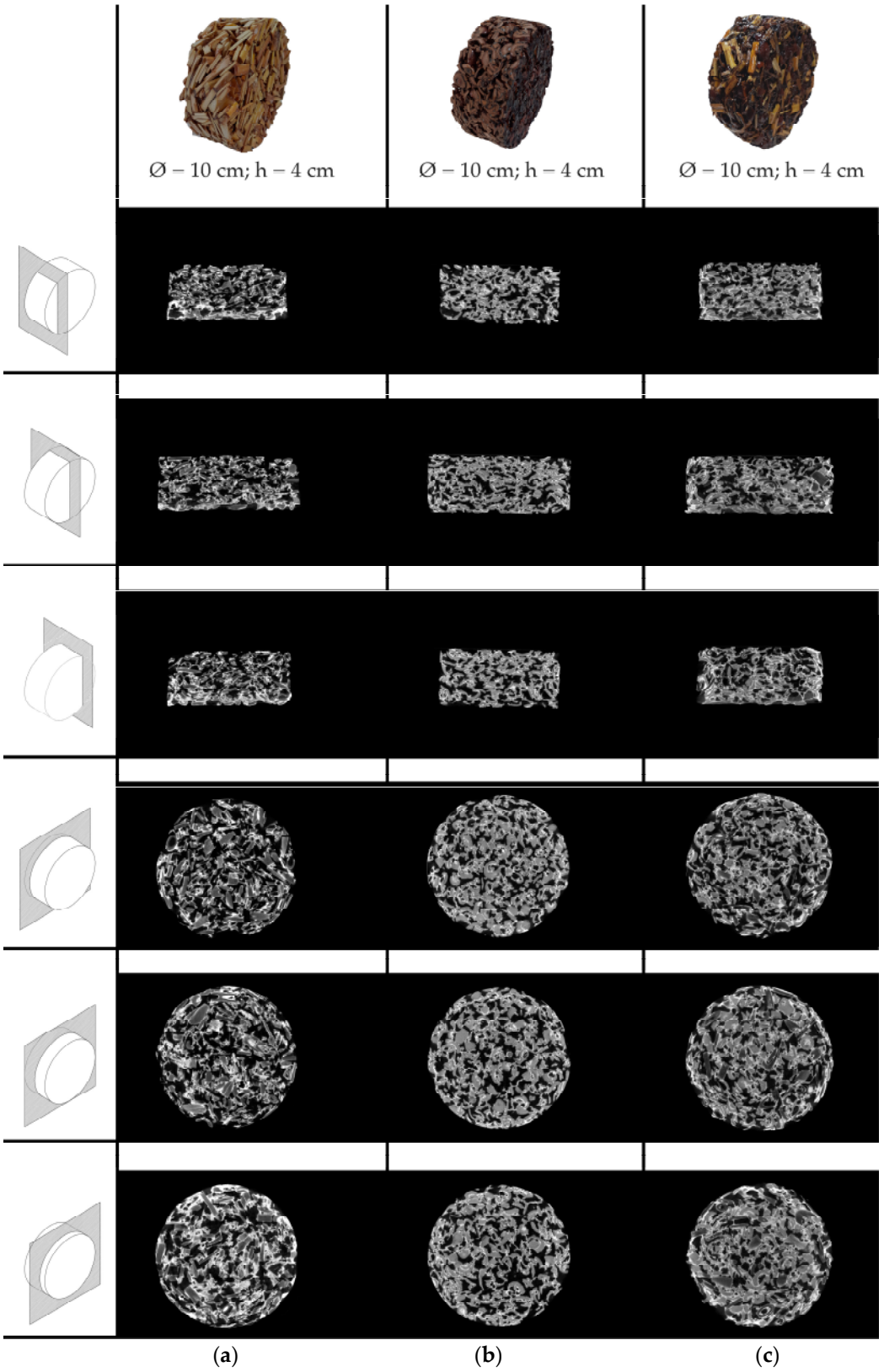

Figure 5. Cylindrical samples of each composite and their corresponding internal structures (transverse and longitudinal sections): (**a**) *A. donax*-based composite; (**b**) hazelnut-shell-based composite; and (**c**) mixture-based composite.

The differences between the internal structures of the composites were more pronounced along their thickness (h = 4 cm). The hazelnut-shell-based samples seemed more homogeneous than the *A. donax*-based ones. For these, the sodium silicate (the white parts in Figure 5) was mainly on the bottom side (the one in contact with the mold during the production process). This is in line with the expectation, as the optimization of the production process was defined by considering hazelnut shells [31]. Furthermore, the differences between samples were coherent with the values of the standard deviation of the apparent density (Section 4.1).

Evident differences were found between the shapes of voids and aggregates, which determined different internal connections. The contribution of the sodium silicate solution's distribution significantly affected the type of porosity. As represented in Mati-Baouche et al.'s study [68], the combination of the adhesive–aggregate produced solid, closed pores, open pores, dead-end pores, dead-end clusters, and, hence, kinematic porosity, and dead-end porosity (properties mainly considered in the acoustic field).

Table 3 reports the results of the internal porosity of each composite sample, the average values, and the standard deviation (SD).

The composites showed similar percentages of solids/voids, with a variation of only 5%. Hence, the porosity seemed to be determined by the mixture of the bio-aggregate–adhesive rather than by the type of bio-aggregate. The latter seemed to influence mainly the shape and size of voids, their connections, and the tortuosity. The standard deviation related to the average value was low (with a maximum of 5%). Hence, the reproducibility was good: similar results were achieved for the three replications.

The evaluated porosity was considered "macroporosity" as the percentage of macropores, determined by the arrangement of the shredded bio-aggregates [62,68], was provided. The large sizes of pores were determined by the aggregate grain size, between 4 and 8 mm (Section 2.1). Further analysis could be performed to define the other types of porosity, as discussed in Section 4.5.

The quantification of the percentages of solids/voids was a starting point for the analysis of further characteristics of the internal structures of the samples. Certainly, in addition to the number of voids, their shapes, their connections, and the tortuosity influenced the final performance of the composites, as discussed in the following sections.

4.3. Hygroscopicity Properties

Figure 6 shows the moisture adsorption/desorption content curves of the materials for four adsorption/desorption cycles. Three samples for each aggregate (i.e., three samples of *A. donax* (AA), three of hazelnut shells (HH), and three of the mixture of *A. donax* and hazelnut shells (AAHH)), and four samples of sodium silicate (S) were considered and reported. To provide a clearer representation, the same color and style of lines were considered for the same tested material.

The differences between the moisture content values for each material become more marked along the cycles. Indeed, at the beginning of the test (12 h and 24 h), the curves achieved values that varied within ± 0.03 kg/m^2; at the end (84 h and 96 h), the range increased (± 0.06 kg/m^2). As for the curves, all the materials showed similar behavior. *A. donax* (both alone and mixed with the hazelnut shells) stabilized earlier than the others, having similar values during the four testing days. Meanwhile, for both the hazelnut shells and the dried sodium silicate solution, the curve increased during the test, demonstrating a higher moisture storage capacity, more markedly for the sodium silicate. Indeed, the sodium silicate solution achieved the highest values of moisture adsorption and desorption content for all cycles, followed by the hazelnut shells, and then by *A. donax* and the mixture of the two aggregates. These results are in line with the expectation, as sodium silicate is known to be highly hygroscopic [44,48].

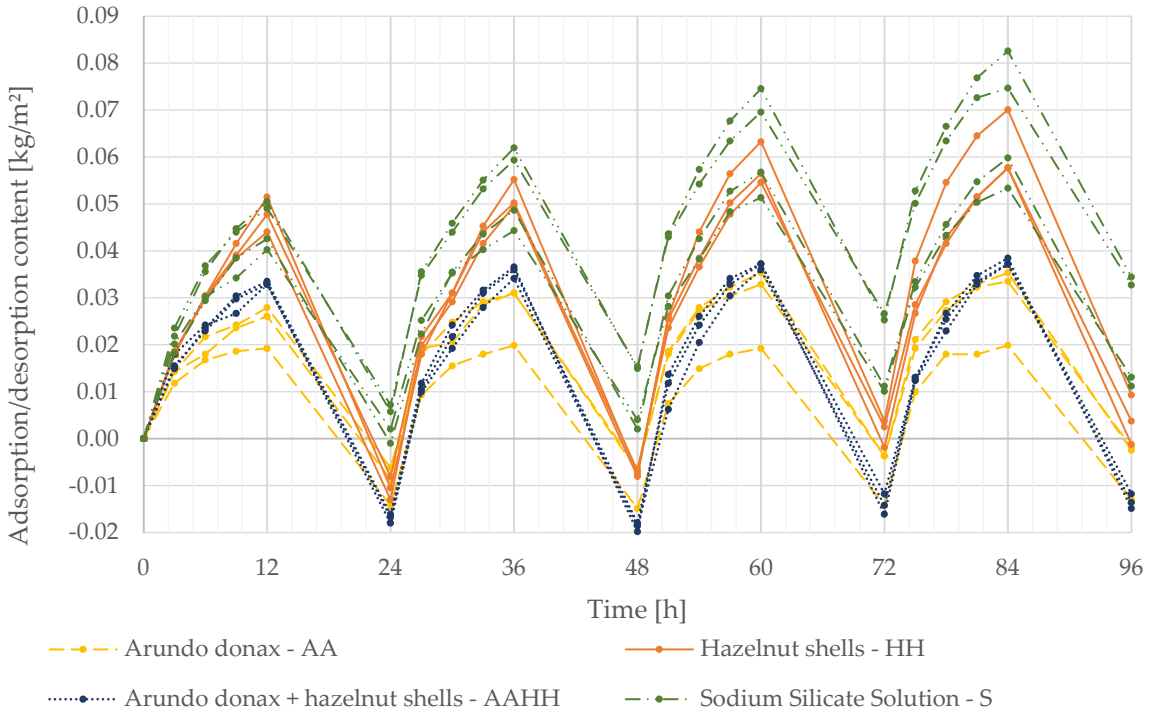

Figure 6. Moisture adsorption/desorption contents for four cycles of three samples of each bio-aggregate and four samples of the sodium silicate solution, considered separately.

Considering the values of moisture adsorption ($\rho_{A,ac}$) for each cycle (average values), the hazelnut shells achieved the highest values, with a $\rho_{A,ac}$ between 0.048 kg/m^2 and 0.066 kg/m^2. *A. donax* achieved the lowest values, with a $\rho_{A,ac}$ between 0.024 kg/m^2 and 0.038 kg/m^2. The same was found for the moisture desorption content ($\rho_{A,dc}$): the hazelnut shells showed the highest values, with a $\rho_{A,dc}$ between 0.057 kg/m^2 and 0.059 kg/m^2, and *A. donax* showed the lowest ones, with a $\rho_{A,dc}$ between 0.034 kg/m^2 and 0.037 kg/m^2. The moisture content difference, $\rho_{A,sc}$, for the bio-aggregates decreased after the first cycle, differently from the sodium silicate solution, for which the $\rho_{A,sc}$ increased during the test: 0.003 kg/m^2 after the first cycle, 0.006 kg/m^2 after the second, 0.009 kg/m^2 after the third, and, finally, 0.005 kg/m^2. This shows that the sodium silicate stored the moisture, and its sorption capacity increased.

Cintura et al. [28] evaluated the hygroscopicity of some agro-industrial wastes, including hazelnut shells, using the same test method. Although the researchers achieved higher values for both the sorption and desorption moisture content, the trend of the curve was similar, and the hazelnut shells showed a moisture storage capacity. The differences between the values could be determined by the different types of hazelnut shells (their physical and chemical properties) as well as the differences in the employed equipment.

Hygroscopicity is strictly related to the chemical and physical properties of the material, including the porosity [54,62,69], as previously reported (Section 4.2). The results indicate a greater porosity for the hazelnut shells than for *A. donax*, which is different from the expectation. Indeed, the results of the loose bulk density (469 kg/m^3 for hazelnut shells [29] and 181.3 kg/m^3 [30] for *A. donax*) would lead to hypothesize a greater porosity for *A. donax*, as the two properties are correlated [70]. The same for the thermal insulation performance, as *A. donax* demonstrated a promising thermal insulation performance [35,39], and the two properties are strictly connected [60,71]. However, considering only the porosity is too simplifying, as many other parameters affect both the hygroscopicity and the other properties.

As for the dried sodium silicate solution, its high hygroscopicity is derived from its chemical composition. It ensures an easy reaction with water and makes the sodium silicate able to absorb moisture from the environment, as detailed in past research [38,48].

Figure 7 shows the moisture adsorption/desorption content curves during the four cycles for the composite samples (i.e., three samples of the *A. donax*-based composite (A), three of the hazelnut-shell-based one (H), and three of the mixture-based one (AH)). Again, the same color and style of lines were considered for the samples of the same composite.

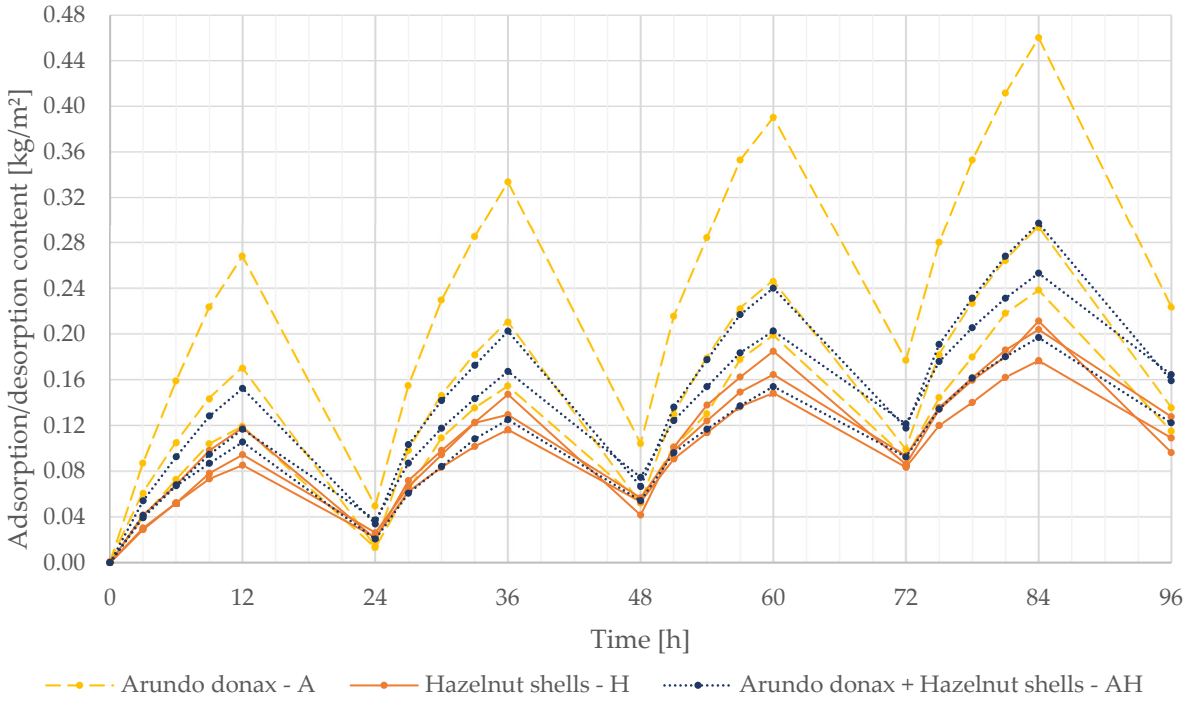

Figure 7. Moisture adsorption/desorption contents for four cycles of three samples for each composite.

The hazelnut-shell-based composite achieved the lowest values of moisture content in the four cycles. The composite made of *A. donax* (both alone and combined) reached the highest values. The hygroscopicity depended on the aggregates, the adhesive, and their coupling [72], as well as the conformation of the composite, namely, the adhesive's distribution, the porosity, and the grain size of the aggregate [73]. For this reason, one of the samples of the *A. donax*-based composite showed different values: the exposed surface could have had a different distribution of the sodium silicate solution or different aggregate grain sizes. However, considering the average curves, the composites showed similar behavior (similar trends in the moisture adsorption/desorption curves).

None of them reached stability after the four cycles, as the adsorption and desorption moisture contents continued to increase. Indeed, considering the average values, the moisture absorption content, $\rho_{A,ac}$, increased from 0.099 kg/m^2 to 0.110 kg/m^2 for the hazelnut-shell-based composite (increasing by 11%); from 0.186 kg/m^2 to 0.208 kg/m^2 for the *A. donax*-based one (increasing by 12%); and from 0.125 kg/m^2 to 0.139 kg/m^2 for the mixture-based one (increasing by 11%). The moisture desorption content, $\rho_{A,dc}$, increased from 0.076 kg/m^2 to 0.087 kg/m^2 for the hazelnut-shell-based composite (increasing by 13%); from 0.160 kg/m^2 to 0.173 kg/m^2 for the *A. donax*-based one (increasing by 8%); and from 0.094 kg/m^2 to 0.101 kg/m^2 for the mixture-based one (increasing by 7%). The moisture content difference, $\rho_{A,sc}$, was between 0.023 kg/m^2 and 0.037 kg/m^2 for the hazelnut-shell-based composite; between 0.026 kg/m^2 and 0.053 kg/m^2 for the *A. donax*-based one; and between 0.031 kg/m^2 and 0.045 kg/m^2 for the mixture-based one. The highest values of moisture content difference were achieved during the third cycle for all composites. After this cycle, the samples started to stabilize.

To investigate in more detail the correlation between the materials and the composites, the average values for all were considered. They are reported in Figure 8.

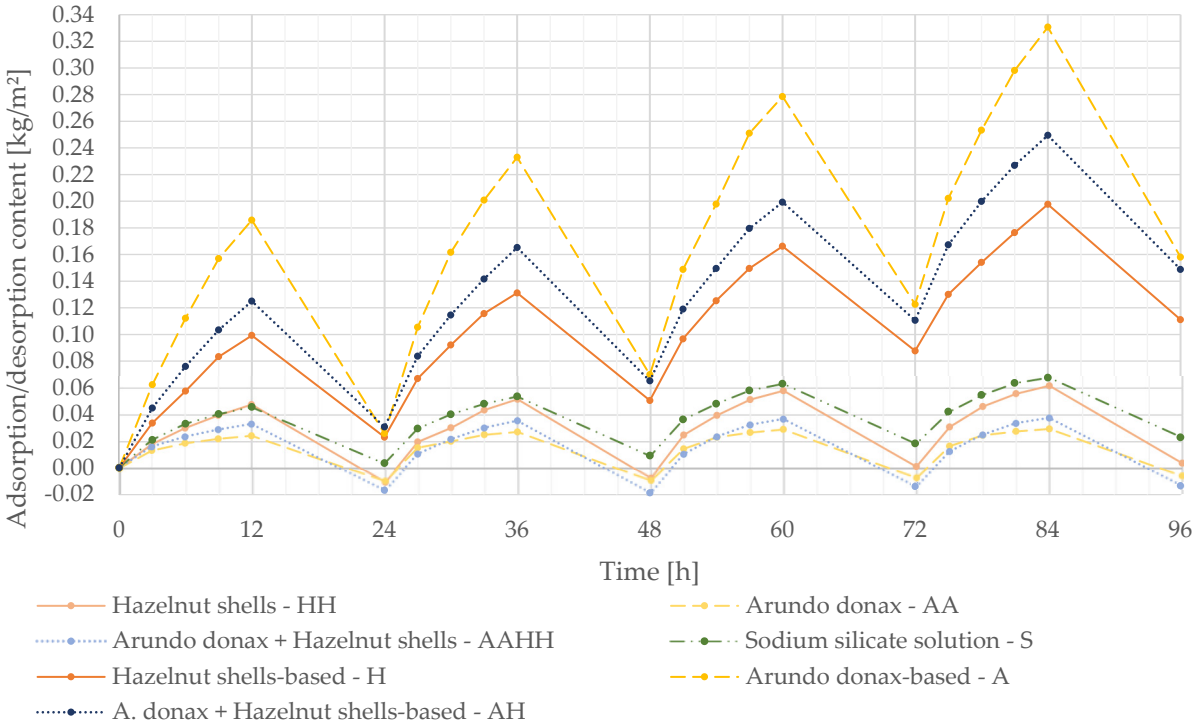

Figure 8. Moisture adsorption/desorption contents for four cycles of the tested samples: comparison between materials and composites (average values).

These results show the strong influence of the sodium silicate on the final performance. Indeed, by adding the sodium silicate solution, the hygroscopicity and the moisture storage capacity of the bio-aggregates strongly increased. For example, as Figure 8 shows, considering the last cycle, from values of moisture content between 0.03 kg/m^2 and 0.06 kg/m^2 after 84 h for the bio-aggregates, the sodium silicate allowed achieving values in the range of 0.20–0.33 kg/m^2 after 84 h. The moisture content difference, $\rho_{A,sc}$, increased, too. This is in line with past studies that demonstrated that the adhesives (binder/glue) strongly affected the final properties of the composites [19,21,60]. The advantage here, in comparison with other more common binders, is that the sodium silicate solution has a significative positive effect on the hygroscopic capacity.

Comparing the hygroscopicity of the raw materials and the composites, there was no correspondence. Indeed, the most hygroscopic raw materials (hazelnut shells) did not produce the most hygroscopic composite (which was the *A. donax*-based one). Hence, a correlation between the aggregates and composites cannot be defined. This was caused by the combination of the sodium silicate–aggregate, in particular, by the different sodium silicate distributions on the exposed surfaces. Indeed, according to Figure 5, the *A. donax*-based samples had a greater amount of sodium silicate on one side, and this could have significantly affected their hygroscopic behavior. The results and the practical experience suggest that the greater the surface area covered by sodium silicate, the greater the capacity to absorb moisture. Furthermore, the mismatch between the materials and composites demonstrates, again, the strong influence of the adhesive on the performance of the final composites. It is important to underline that the sodium silicate distribution in the composites was assessed only qualitatively, and further analysis should be carried out. However, the results already indicate this correlation between the two properties.

Table 4 reports the moisture buffering values and the classification, following Rode et al. [64], for both the materials—considering the aggregates and adhesive individually—and the composites (with the average values of the last three cycles and standard deviation), calculated as described in Equations (4) and (5) (Section 3.3).

Table 4. Moisture buffering values (MBVs) of the materials and composite samples, considering the average values and standard deviations (SDs) of the three samples for each material/composite.

Samples	MBV (g/(m^2%RH))	Classification (Rode et al. [64])
Materials		
A. donax—AA	1.47 ± 0.04	Good
Hazelnut shells—HH	2.41 ± 0.14	Excellent
Mixture—AAHH	2.11 ± 0.03	Excellent
Sodium silicate—S	1.92 ± 0.18	Good
Composites		
A. donax—A	7.44 ± 1.25	Excellent
Hazelnut shells—H	3.86 ± 0.83	Excellent
Mixture—AH	4.65 ± 1.12	Excellent

Considering the materials, both the *A. donax* and the dried sodium silicate solution were rated as good. Hence, they had lower MBVs than the hazelnut shells. Coherently, the addition of *A. donax* to the hazelnut shells resulted in a lower MBV. As for the sodium silicate result, a higher value of MBV was expected. However, this result was evaluated by considering the average values between the MBV_a and MBV_d of the last three cycles. Considering these separately, the MBV of the sodium silicate solution was MBV_a = 2.05 ± 0.10 g/(m^2%RH) and MBV_d = 1.79 ± 0.01 g/(m^2%RH). Hence, as expected, the MBV of the sorption phase was higher than that of the desorption phase (Table 4 reports its average value).

The MBVs of the composites are coherent with the previous results (Figure 7). Again, the values of *A. donax* were influenced by the distribution of the sodium silicate, which determined higher values. As for the mixture, the results are in line with the expectation: the combination of the two materials determined a lowering of the moisture buffering capacity, and then of the MBV.

4.4. Statistical Analysis

Table 5 summarizes the results of the ANOVA (reporting F- and *p*-values).

Table 5. Results of ANOVA (F- and *p*-values) considering raw materials as the variable.

Property	F	*p*-Value
Apparent density	9.53	0.013739
MBV *	9.33	0.008070
Porosity	5.15	0.049987

* Note: For MBV, both the materials (individually) and the composites were considered as the variable.

The statistical analysis showed that considering the materials as the variable, the alternative hypothesis was confirmed (F < 1; the *p*-value was less than 0.05; and the H0 was false, as described in Section 3.4) for all. Hence, at least one of the groups was different.

Table 6 reports the *p*-values of the post hoc tests, defining where the differences were. Indeed, the *p*-values allowed identifying which and how the groups were significantly different from each other. The first two columns show which groups were compared with each other, considering the three composites (A, H, and AH) for all the properties, and also the materials individually (AA, HH, and AAHH) for the hygroscopicity. For easy reading of the results, when the materials (individually) are compared with each other, the results are underlined; when they are compared with the composites, they are underlined. *A. donax* is not reported in italics to avoid any confusion.

Table 6. *p*-values of the post hoc tests for the results that were significant (considering adhesives as the variable).

Group A	Group B	*p*-Value *
Apparent Density		
A. donax-based composite—A	**Hazelnut-shell-based composite—H**	**0.012**
A. donax-based composite—A	Mixture-based composite—AH	0.066
Hazelnut-shell-based composite—H	Mixture-based composite—AH	0.380
MBV		
A. donax-based composite—A	**Hazelnut-shell-based composite—H**	**0.038**
A. donax-based composite—A	Mixture-based composite—AH	0.136
Hazelnut-shell-based composite—H	Mixture-based composite—AH	0.968
A. donax (raw material)—AA	Hazelnut shells (raw material)—HH	0.932
A. donax (raw material)—AA	Mixture (raw material)—AAHH	0.987
Hazelnut shells (raw material)—HH	Mixture (raw material)—AAHH	1.000
Hazelnut shells (raw material)—HH	***A. donax-based composite—A***	***0.004***
Hazelnut shells (raw material)—HH	*Hazelnut-shell-based composite—H*	*0.709*
Hazelnut shells (raw material)—HH	*Mixture-based composite—AH*	*0.305*
Mixture (raw material)—AAHH	***A. donax-based composite—A***	***0.002***
Mixture (raw material)—AAHH	*Hazelnut-shell-based composite—H*	*0.539*
Mixture (raw material)—AAHH	*Mixture-based composite—AH*	*0.198*
A. donax (raw material)—AA	***A. donax-based composite—A***	***0.001***
A. donax (raw material)—AA	*Hazelnut-shell-based composite—H*	*0.244*
A. donax (raw material)—AA	*Mixture-based composite—AH*	*0.074*
Porosity		
A. donax-based composite—A	Hazelnut-shell-based composite—H	0.405
A. donax-based composite—A	Mixture-based composite—AH	0.244
Hazelnut-shell-based composite—H	**Mixture-based composite—AH**	**0.043**

* Note: The numbers in bold represent *p*-values of less than 0.05; underlined results represent materials (individually) compared with each other; and italicized results represent materials (individually) compared with the composites.

p-values of less than 0.05 (highlighted in bold in Table 6) indicated which groups were significantly different. Both for the apparent density and MBV, the results for the *A. donax*-based and hazelnut-shell-based composites defined two distinguishable groups. As for the porosity, a significant difference was found between the hazelnut-shell-based composite and the mixture-based one. This confirms the observations reported in the previous section (Section 4.2): the porosity was determined more by the combination of the sodium silicate–aggregate than by the type of aggregate.

Considering the comparisons between the raw materials for the MBV (the underlined values in Table 6), they did not determine distinguishable groups (the *p*-values were always higher than 0.05). As for the comparison between the materials and composites (values reported in italics in Table 6), significant differences were always found between the materials (AA, HH, and AAHH) and the *A. donax*-based composite (A). This suggests that for the *A. donax*-based composite, the sodium silicate solution strongly influenced the final performance. This is in line with the previous results, both for hygroscopicity and internal structure (Figure 5).

4.5. Additional Discussion

In addition to the considerations and comparisons carried out in the previous sections, further discussions were conducted. These ensured a better understanding of the composites' properties and materials' contributions. Moreover, the benefits and drawbacks of the studied composites were pointed out, as well as their possible applications.

Considering the apparent density, as the addition of *A. donax* lowered the results of the hazelnut-shell-based composite, this could probably improve the insulation thermal

properties, too. Density and thermal conductivity are strictly correlated [74,75]. However, this consideration should be verified.

Hygroscopicity, porosity, and internal structure are strictly connected. The porosity includes a large range of pore sizes: macropores derived from the bio-aggregates' arrangement, mesopores within the aggregates and the adhesive, and the micropores of the aggregates and the adhesive. Even if the present study considered only the macroporosity, all these porosities affected the moisture storage capacity, together with the ratio of the aggregate/adhesive and the grain size [62,70]. The moisture sorption/desorption capacity also depends on the surface area available for vapor exchange and other hygroscopic properties [73].

The porosity and the information about the internal structure could provide a better understanding of many other properties, too. They are strictly connected to the final performance of the composite. In addition to the hygroscopicity [62], they could influence the sound absorption and thermal insulation [76,77].

Considering all the results, it was confirmed that the hygroscopicity depended on both the aggregates and the sodium silicate. The latter more significantly affected the moisture storage capacity. As the percentages of the aggregate–adhesive were the same for all samples, the differences in the results were mainly caused by the sodium silicate distribution. This changed due to the types of aggregates, namely, their physical and chemical properties and their reactions with the adhesive. The statistical analysis confirmed these considerations. For the MBV, the distinguishable groups (Table 6) were the composites with *A. donax* and the sodium silicate solution. According to Figure 5, these composites showed less homogeneity and a higher amount of sodium silicate on one side of the samples (Section 4.2).

Bio-aggregates are known to be highly porous and, hence, highly hygroscopic. Knowing their internal structures, too, is useful to understand their properties even better [54]. However, other types of analysis are more suitable for this purpose, such as scanning electron microscopy (SEM), mercury intrusion porosimetry (MIP), and sorption techniques. Future studies could consider these laboratory tests to investigate the correlation between these properties on a micro-scale.

High hygroscopicity could be both an advantage and a drawback. Indeed, hygroscopic building materials and products can passively contribute to the control of indoor conditions [61] and can secure indoor hygrothermal comfort and better indoor air quality [78,79], which are extremely important for human health and users' well-being [80]. On the other hand, a high moisture storage capacity and moisture content could determine the material's degradation [24]. Furthermore, bio-based composites can be easily attacked by microorganisms due to their chemical composition, their organic nature, and their pH [81,82]. Apart from the aesthetic impact, a biological attack can lower the durability of composites, affect the materials' properties, and restrict their performance, modify their chemical compositions, and compromise their natural structures [83]. Furthermore, biological degradation can affect human health, causing diseases and lowering indoor air quality [84,85].

However, sodium silicate has demonstrated good resistance to biological attack [21] and is known to avoid mold growth and material decomposition [45–47]. The present study confirmed this property, as no biological colonization was detected after the hygroscopicity test. Moreover, as moisture storage can be crucial, determining the critical moisture level [86,87] could be useful to better define this possible drawback and moderate it. Furthermore, some strategies could improve low moisture resistance, such as the addition of additives, such as phosphorus, boron, or silica fume [48].

The results suggest that the hazelnut-shell-based and *A. donax*-based composites could be employed as indoor coating boards, passively regulating internal conditions, hygrothermal comfort, and energy demand [73,88,89]. These types of building composites could also be useful for the preservation of architectural heritage, namely, vernacular buildings. Being bio-based, the employed materials would be compatible with vernacular architecture's typical materials. Their high hygroscopicity and moisture buffering capacity

would avoid the creation of water vapor barriers, which is crucial to avoid wall and roof degradation. Moreover, by knowing these types of composites' behaviors, other possibilities could be proposed, which could be suitable for historic architectural heritage, too. A possible effective solution for the bio-based composites could be a superficial application of the sodium silicate solution to both protect the bio-based materials and secure the passive control of indoor hygroscopic conditions. However, this is an idea for future studies, suggested by the analysis of the present study, which should be investigated and confirmed.

5. Conclusions

The present study analyzed *A. donax*-based and hazelnut-shell-based boards produced using a sodium silicate solution as the adhesive. The performed laboratory tests considered their apparent density, internal structure, porosity, and hygroscopicity. The connection between the composites and the materials' properties and the influence of the distributions of the aggregates and the adhesive were considered, too. Indeed, this research work wanted to investigate the correlation between the final performance of the boards and the contribution of each composing material.

The results allowed the achievement of the following conclusions:

- The hazelnut-shell-based composite had a higher apparent density than the *A. donax*-based one. Therefore, the addition of *A. donax* to the mixture of hazelnut shells and the sodium silicate solution lowered the apparent density. Hence, it could probably improve the thermal performance, too. The results of the replications and the values of standard deviation confirm the good homogeneity between the samples of each composite.
- The tomography enabled knowing the internal structures of the composites. A qualitative evaluation suggested a better homogeneity in the hazelnut-shell-based composite. In the *A. donax*-based composite, the sodium silicate solution was deposited more on one side of the sample (the bottom face). This could affect the final performance, such as the moisture storage capacity.
- The tomography allowed defining the porosity, too. The results demonstrate that this property was mainly determined by the contents of the selected materials (the bio-aggregates and adhesive) rather than by the type of bio-aggregate. The latter affected the type of voids (size and shape) and the sodium silicate distribution.
- Both the materials and the composites were highly hygroscopic, as expected. The addition of the sodium silicate solution increased the hygroscopicity and the moisture storage capacity. Furthermore, the sodium silicate's distribution in the samples significantly influenced their final performance, and this caused a mismatching between the results of the materials and composites. These results were confirmed by the statistical analysis (ANOVA).

The correlations between the properties of the materials (individually) and the composites were defined. Knowing which and how these parameters could influence the final performance is extremely helpful for their optimization and future research development. The strong influence of the adhesive content on the final properties was confirmed, as well as the high hygroscopicity of the considered composites. The results suggest that in the case of the employment of the composites as internal coating boards, they could passively control indoor hygrothermal comfort. This could improve both indoor conditions and internal comfort and lower energy demands. Furthermore, when considered as bio-based boards, they could be compatible with the elements in vernacular architecture. Hence, starting from this research study, useful solutions for the preservation of cultural architectural heritage could be developed.

Author Contributions: Conceptualization, E.C., L.N., L.M. and P.F.; methodology, E.C. and M.B.; software, R.B.; validation, E.C. and M.B.; formal analysis, E.C. and M.B.; investigation, E.C.; resources, M.B., R.B. and M.P.M.; data curation, E.C.; writing—original draft preparation, E.C.; writing—review and editing, L.N., L.M., P.F. and M.B.; visualization, E.C.; supervision, L.N., L.M. and P.F.; project administration, L.N. and P.F.; funding acquisition, L.N. and P.F. All authors have read and agreed to the published version of the manuscript.

Funding: This research was funded by the Portuguese Foundation for Science and Technology (FCT), with the Ph.D. grant PD/BD/150579/2020 of the first author, as part of the Eco-Construction and Rehabilitation Program (EcoCoRe). The authors are grateful for the FCT's support through their funding (UIDB/04625/2020) of the research unit CERIS, and for EU funding of Erasmus+ project Bio-fibre (2022-1-DK01-KA220-HED-000086641).

Data Availability Statement: The raw data supporting the conclusions of this article will be made available by the authors on request.

Acknowledgments: The authors acknowledge the technicians of the LISG and DIN Labs of the University of Bologna for their help in the laboratory tests; Silvio Salvi and Daniele Rabboni (Department of Agricultural and Food Sciences, University of Bologna, Italy) for providing *A. donax*; Luca Barbaresi for making available the equipment to carry out the hygroscopicity tests. The authors would like to thank Lorenzo Coraglia (Raccolti di CIN) for donating the hazelnut shells to carry out this research and for the information about this crop's production; Mirko Braga (Ingessil S.r.l) for providing the sodium silicate solution and his help and suggestion to use it; and Stefania Liuzzi (the Polytechnic University of Bari) for providing suggestions to carry out this research.

Conflicts of Interest: The authors declare no conflicts of interest.

References

1. European Commission. *The Europen Green Deal—Comunication from the Commission to the European Parliament, the European Council, the Council, the European Economic and Social Committee and the Committee of the Regions*; European Commission: Brussels, Belgium, 2019.
2. Posani, M.; Veiga, R.; de Freitas, V.P. Retrofitting Historic Walls: Feasibility of Thermal Insulation and Suitability of Thermal Mortars. *Heritage* **2021**, *4*, 2009–2022. [CrossRef]
3. Martínez-García, C.; González-Fonteboa, B.; Carro-López, D.; Pérez-Ordóñez, J.L. Mussel Shells: A Canning Industry by-Product Converted into a Bio-Based Insulation Material. *J. Clean. Prod.* **2020**, *269*, 122343. [CrossRef]
4. Onu Agenda 2030. Available online: https://unric.org/en/united-nations-sustainable-development-goals/ (accessed on 13 October 2023).
5. Caponetto, R.; Cuomo, M.; Detommaso, M.; Giuffrida, G.; Lo Presti, A.; Nocera, F. Performance Assessment of Giant Reed-Based Building Components. *Sustainability* **2023**, *15*, 2114. [CrossRef]
6. Binici, H.; Aksogan, O. Eco-Friendly Insulation Material Production with Waste Olive Seeds, Ground PVC and Wood Chips. *J. Build. Eng.* **2016**, *5*, 260–266. [CrossRef]
7. Liuzzi, S.; Sanarica, S.; Stefanizzi, P. Use of Agro-Wastes in Building Materials in the Mediterranean Area: A Review. *Energy Procedia* **2017**, *126*, 242–249. [CrossRef]
8. Salonen, T.; Fischer, H.; Korjenic, A. Chopped Straw as an Insulation Material: The Influence of Different Blow-in Technologies and Flame Retardants on Hygrothermal Properties. *Buildings* **2023**, *13*, 2555. [CrossRef]
9. Palumbo, M.; Navarro, A.; Giraldo, P.; Lesar, B.; Lacasta, A.M. Performance of Biobased Insulation Board from Crop Byproducts and Natural Gums. *Acad. J. Civ. Eng.* **2015**, *33*, 189–196.
10. Embirsh, H.S.A.; Stajčić, I.; Gržetić, J.; Mladenović, I.O.; Anđelković, B.; Marinković, A.; Vuksanović, M.M. Synthesis, Characterization and Application of Biobased Unsaturated Polyester Resin Reinforced with Unmodified/Modified Biosilica Nanoparticles. *Polymers* **2023**, *15*, 3756. [CrossRef]
11. Nadhari, W.N.A.W.; Danish, M.; Nasir, M.S.R.M.; Geng, B.J. Mechanical Properties and Dimensional Stability of Particleboard Fabricated from Steam Pre-Treated Banana Trunk Waste Particles. *J. Build. Eng.* **2019**, *26*, 100848. [CrossRef]
12. Auriga, R.; Pędzik, M.; Mrozowski, R.; Rogoziński, T. Hemp Shives as a Raw Material for the Production of Particleboards. *Polymers* **2022**, *14*, 5308. [CrossRef]
13. Carneiro, P.; Jerónimo, A.; Silva, V.; Cartaxo, F.; Faria, P. Improving Building Technologies with a Sustainable Strategy. *Procedia-Soc. Behav. Sci.* **2016**, *216*, 829–840. [CrossRef]
14. Liuzzi, S.; Rubino, C.; Stefanizzi, P.; Petrella, A.; Boghetich, A.; Casavola, C.; Pappalettera, G. Hygrothermal Properties of Clayey Plasters with Olive Fibers. *Constr. Build. Mater.* **2018**, *158*, 24–32. [CrossRef]
15. Ferreira, A.M.; Pereira, J.; Almeida, M.; Ferra, J.; Paiva, N.; Martins, J.; Magalhães, F.D.; Carvalho, L.H. Low-Cost Natural Binder for Particleboards Production: Study of Manufacture Conditions and Stability. *Int. J. Adhes. Adhes.* **2019**, *93*, 102325. [CrossRef]

16. Saman, N.S.M.; Deraman, R.; Hamzah, M.H. Development of Low Thermal Conductivity Brick Using Rice Husk, Corn Cob and Waste Tea in Clay Brick Manufacturing. *AIP Conf. Proc.* **2017**, *1901*, 130007. [CrossRef]
17. Savic, A.; Antonijevic, D.; Jelic, I.; Zakic, D. Thermomechanical Behavior of Bio-Fiber Composite Thermal Insulation Panels. *Energy Build.* **2020**, *229*, 110511. [CrossRef]
18. Eschenhagen, A.; Raj, M.; Rodrigo, N.; Zamora, A.; Labonne, L.; Evon, P.; Welemane, H. Investigation of Miscanthus and Sunflower Stalk Fiber-Reinforced Composites for Insulation Applications. *Adv. Civ. Eng.* **2019**, *2019*, 9328087. [CrossRef]
19. Younesi-Kordkheili, H.; Pizzi, A. Improving the Physical and Mechanical Properties of Particleboards Made from Urea–Glyoxal Resin by Addition of PMDI. *Eur. J. Wood Wood Prod.* **2018**, *76*, 871–876. [CrossRef]
20. Solt, P.; Konnerth, J.; Gindl-Altmutter, W.; Kantner, W.; Moser, J.; Mitter, R.; van Herwijnen, H.W.G. Technological Performance of Formaldehyde-Free Adhesive Alternatives for Particleboard Industry. *Int. J. Adhes. Adhes.* **2019**, *94*, 99–131. [CrossRef]
21. Cintura, E.; Faria, P.; Duarte, M.; Nunes, L. Eco-Efficient Boards with Agro-Industrial Wastes—Assessment of Different Adhesives. *Constr. Build. Mater.* **2023**, *404*, 132665. [CrossRef]
22. Antov, P.; Savov, V.; Mantanis, G.I.; Neykov, N. Medium-Density Fibreboards Bonded with Phenol-Formaldehyde Resin and Calcium Lignosulfonate as an Eco-Friendly Additive. *Wood Mater. Sci. Eng.* **2020**, *16*, 42–48. [CrossRef]
23. Owodunni, A.A.; Lamaming, J.; Hashim, R.; Taiwo, O.F.A.; Hussin, M.H.; Mohamad Kassim, M.H.; Bustami, Y.; Sulaiman, O.; Amini, M.H.M.; Hiziroglu, S. Adhesive Application on Particleboard from Natural Fibers: A Review. *Polym. Compos.* **2020**, *41*, 4448–4460. [CrossRef]
24. Palumbo, M.; Lacasta, A.M.; Navarro, A.; Giraldo, M.P.; Lesar, B. Improvement of Fire Reaction and Mould Growth Resistance of a New Bio-Based Thermal Insulation Material. *Constr. Build. Mater.* **2017**, *139*, 531–539. [CrossRef]
25. Tobon, A.M.; Andres, Y.; Locoge, N. Impacts of Test Methods on the Assessment of Insulation Materials' Resistance against Moulds. *Build. Environ.* **2020**, *179*, 106963. [CrossRef]
26. Liu, L.; Li, H.; Lazzaretto, A.; Manente, G.; Tong, C.; Liu, Q.; Li, N. The Development History and Prospects of Biomass-Based Insulation Materials for Buildings. *Renew. Sustain. Energy Rev.* **2017**, *69*, 912–932. [CrossRef]
27. Viel, M.; Collet, F.; Lanos, C. Chemical and Multi-Physical Characterization of Agro-Resources' by-Product as a Possible Raw Building Material. *Ind. Crops Prod.* **2018**, *120*, 214–237. [CrossRef]
28. Cintura, E.; Faria, P.; Duarte, M.; Nunes, L. Bio-Wastes as Aggregates for Eco-Efficient Boards and Panels: Screening Tests of Physical Properties and Bio-Susceptibility. *Infrastructures* **2022**, *7*, 26. [CrossRef]
29. Cintura, E.; Faria, P.; Molari, L.; Barbaresi, L.; D'Orazio, D.; Nunes, L. A Feasible Re-Use of an Agro-Industrial by-Product: Hazelnut Shells as High-Mass Bio-Aggregate in Boards for Indoor Applications. *J. Clean. Prod.* **2024**, *434*, 140297. [CrossRef]
30. Cintura, E.; Faria, P.; Molari, L.; Barbaresi, L.; D'Orazio, D.; Nunes, L. Characterization of an *Arundo Donax*-Based Composite: A Solution to Improve Indoor Comfort. *Ind. Crops Prod.* **2024**, *208*, 117756. [CrossRef]
31. Cintura, E.; Faria, P.; Molari, L.; Nunes, L. Optimisation of Production Parameters to Develop Innovative Eco-Efficient Boards. In *Bio-Based Building Materials Proceedings of ICBBM 2023*; Amziane, S., Merta, I., Page, J., Eds.; Springer: Cham, Switzerland, 2023; pp. 111–122; ISBN 9783031334641.
32. Çöpür, Y.; Güler, C.; Akgül, M.; Taşçıoğlu, C. Some Chemical Properties of Hazelnut Husk and Its Suitability for Particleboard Production. *Build. Environ.* **2007**, *42*, 2568–2572. [CrossRef]
33. Lopes, L.P.C.; Martins, J.; Esteves, B.; Lemos, L.T.D.E. New Products from Hazelnut Shell. In Proceedings of the ECOWOOD 2012—5th International Conference on Environmentally-Compatible Forest Products, Porto, Portugal, 5–7 September 2012; pp. 83–90.
34. Cintura, E.; Nunes, L.; Esteves, B.; Faria, P. Agro-Industrial Wastes as Building Insulation Materials: A Review and Challenges for Euro-Mediterranean Countries. *Ind. Crops Prod.* **2021**, *171*, 113833. [CrossRef]
35. Barreca, F.; Martinez Gabarron, A.; Flores Yepes, J.A.; Pastor Pérez, J.J. Innovative Use of Giant Reed and Cork Residues for Panels of Buildings in Mediterranean Area. *Resour. Conserv. Recycl.* **2019**, *140*, 259–266. [CrossRef]
36. García-Ortuño, T.; Andréu-Rodríguez, J.; Ferrández-García, M.T.; Ferrández-Villena, M.; Ferrández-García, C.E. Evaluation of the Physical and Mechanical Properties of Particleboard Made from Giant Reed (*Arundo donax* L.). *BioResources* **2011**, *6*, 477–486. [CrossRef]
37. Malheiro, R.; Ansolin, A.; Guarnier, C.; Fernandes, J.; Amorim, M.T.; Silva, S.M.; Mateus, R. The Potential of the Reed as a Regenerative Building Material—Characterisation of Its Durability, Physical, and Thermal Performances. *Energies* **2021**, *14*, 4276. [CrossRef]
38. Liu, S.; Ott, W.K. Sodium Silicate Applications in Oil, Gas & Geothermal Well Operations. *J. Pet. Sci. Eng.* **2020**, *195*, 107693. [CrossRef]
39. Bakatovich, A.; Gaspar, F.; Boltrushevich, N. Thermal Insulation Material Based on Reed and Straw Fibres Bonded with Sodium Silicate and Rosin. *Constr. Build. Mater.* **2022**, *352*, 129055. [CrossRef]
40. Chai, W.; Zhang, L.; Li, W.; Zhang, M.; Huang, J.; Zhang, W. Preparation of Plastics-and Foaming Agent-Free and Porous Bamboo Charcoal Based Composites Using Sodium Silicate as Adhesives. *Materials* **2021**, *14*, 2468. [CrossRef]
41. Zhang, Z.; Chen, H.; Wang, Y.; Wang, G.; Li, L.; Zhong, M.; Bai, H. Effect of Sodium Silicate Binder on the Performance of Ceramic Coatings on Copper Prepared by the Slurry Method. *Surf. Coat. Technol.* **2022**, *448*, 128868. [CrossRef]
42. Rajan, H.S.; Kathirvel, P. Sustainable Development of Geopolymer Binder Using Sodium Silicate Synthesized from Agricultural Waste. *J. Clean. Prod.* **2021**, *286*, 124959. [CrossRef]

43. Kanagaraj, B.; Anand, N.; Samuvel Raj, R.; Lubloy, E. Performance Evaluation on Engineering Properties of Sodium Silicate Binder as a Precursor Material for the Development of Cement-Free Concrete. *Dev. Built Environ.* **2022**, *12*, 100092. [CrossRef]
44. Liu, W.; Xi, W.; Hu, R.; Yue, M.; Yin, Y.; Guo, J.; Zhang, D.; Zhang, H. Preparation and Characterization of Sodium Silicate/Epoxy Resin Composite Bonded Nd-Fe-B Magnets with High Performance. *J. Rare Earths* **2019**, *37*, 1083–1087. [CrossRef]
45. Lee, S.J.; Thole, V. Investigation of Modified Water Glass as Adhesive for Wood and Particleboard: Mechanical, Thermal and Flame Retardant Properties. *Eur. J. Wood Wood Prod.* **2018**, *76*, 1427–1434. [CrossRef]
46. Liuzzi, S.; Rubino, C.; Martellotta, F.; Stefanizzi, P.; Casavola, C.; Pappalettera, G. Characterization of Biomass-Based Materials for Building Applications: The Case of Straw and Olive Tree Waste. *Ind. Crops Prod.* **2020**, *147*, 112229. [CrossRef]
47. Li, L.; Tang, X.; Ouyang, Q.; Tao, N. Combination of Sodium Dehydroacetate and Sodium Silicate Reduces Sour Rot of Citrus Fruit. *Postharvest Biol. Technol.* **2019**, *151*, 19–25. [CrossRef]
48. Song, L.; Liu, W.; Xin, F.; Li, Y. Study of Adhesion Properties and Mechanism of Sodium Silicate Binder Reinforced with Silicate Fume. *Int. J. Adhes. Adhes.* **2021**, *106*, 102820. [CrossRef]
49. Liuzzi, S.; Rigante, S.; Ruggiero, F.; Stefanizzi, P. Straw Based Materials for Building Retrofitting and Energy Efficiency. *Key Eng. Mater.* **2016**, *678*, 50–63. [CrossRef]
50. Ranesi, A.; Posani, M.; Veiga, R.; Faria, P. A Discussion on Winter Indoor Hygrothermal Conditions and Hygroscopic Behaviour of Plasters in Southern Europe. *Infrastructures* **2022**, *7*, 38. [CrossRef]
51. Posani, M.; Vera, V.; Pietro, O.; Brumaud, C.; Dillenburger, B.; Guillaume, H. Re-Thinking Indoor Humidity Control Strategies: The Potential of Additive Manufacturing with Low-Carbon, Super Hygroscopic Materials. *Nat. Commun.* **2023**. *submitted*. [CrossRef]
52. Albertin, F.; Morigi, M.P.; Bettuzzi, M.; Brancaccio, R.; Macchioni, N.; Saccuman, R.; Quarta, G.; Calcagnile, L.; Picchi, D. X-Ray Tomography Unveils the Construction Technique of Un-Montu's Egyptian Coffin (Early 26th Dynasty). *J. Imaging* **2022**, *8*, 39. [CrossRef]
53. Bettuzzi, M.; Casali, F.; Morigi, M.P.; Brancaccio, R.; Carson, D.; Chiari, G.; Maish, J. Computed Tomography of a Medium Size Roman Bronze Statue of Cupid. *Appl. Phys. A* **2015**, *118*, 1161–1169. [CrossRef]
54. Ntimugura, F.; Vinai, R.; Harper, A.; Walker, P. Mechanical, Thermal, Hygroscopic and Acoustic Properties of Bio-Aggregates—Lime and Alkali—Activated Insulating Composite Materials: A Review of Current Status and Prospects for Miscanthus as an Innovative Resource in the South West of England. *Sustain. Mater. Technol.* **2020**, *26*, e00211. [CrossRef]
55. Ratsimbazafy, H.H.; Laborel-Préneron, A.; Magniont, C.; Evon, P. A Review of the Multi-Physical Characteristics of Plant Aggregates and Their Effects on the Properties of Plant-Based Concrete. *Recent Prog. Mater.* **2021**, *3*, 1–69. [CrossRef]
56. Liuzzi, S.; Rubino, C.; Stefanizzi, P.; Martellotta, F. Performance Characterization of Broad Band Sustainable Sound Absorbers Made of Almond Skins. *Materials* **2020**, *13*, 5474. [CrossRef]
57. *EN 323:2002*; Wood-Based Panels—Determination of Density. European Committee for Standardization: Brussels, Belgium, 2002.
58. *ISO 24353:2008*; Hygrothermal Performance of Building Materials and Products-Determination of Moisture Adsorption/Desorption Properties in Response to Humidity Variation. International Organization for Standardization: Geneva, Switzerland, 2008.
59. Brancaccio, R.; Bettuzzi, M.; Casali, F.; Morigi, M.P.; Levi, G.; Gallo, A.; Marchetti, G.; Schneberk, D. Real-Time Reconstruction for 3-D CT Applied to Large Objects of Cultural Heritage. *IEEE Trans. Nucl. Sci.* **2011**, *58*, 1864–1871. [CrossRef]
60. Ansell, M.P.; Lawrence, M.; Jiang, Y.; Shea, A.; Hussain, A.; Calabria-Holley, J.; Walker, P. Natural Plant-Based Aggregates and Bio-Composite Panels with Low Thermal Conductivity and High Hygrothermal Efficiency for Applications in Construction. In *Nonconventional and Vernacular Construction Materials*; Elsevier: Amsterdam, The Netherlands, 2020; pp. 217–245; ISBN 9780081027042.
61. Cascione, V.; Maskell, D.; Shea, A.; Walker, P. A Review of Moisture Buffering Capacity: From Laboratory Testing to Full-Scale Measurement. *Constr. Build. Mater.* **2019**, *200*, 333–343. [CrossRef]
62. Collet, F. *Hygric and Thermal Properties of Bio-Aggregate Based Building Materials*; RILEM State-of-the-Art Reports; Springer: Dordrecht, The Netherlands, 2017; Volume 23, pp. 125–147; ISBN 9789402410310. [CrossRef]
63. Belakroum, R.; Gherfi, A.; Bouchema, K.; Gharbi, A.; Kerboua, Y.; Kadja, M.; Maalouf, C.; Mai, T.H.; El Wakil, N.; Lachi, M. Hygric Buffer and Acoustic Absorption of New Building Insulation Materials Based on Date Palm Fibers. *J. Build. Eng.* **2017**, *12*, 132–139. [CrossRef]
64. Rode, C.; Peuhkuri, R.H.; Mortensen, L.H.; Hansen, K.K.; Time, B.; Gustavsen, A.; Ojanen, T.; Ahonen, J.; Svennberg, K.; Arfvidsson, J.; et al. *Moisture Buffering of Building Materials*; Technical University of Denmark: Kongens Lyngby, Denmark, 2005; ISBN 8778771951.
65. McGregor, F.; Heath, A.; Fodde, E.; Shea, A. Conditions Affecting the Moisture Buffering Measurement Performed on Compressed Earth Blocks. *Build. Environ.* **2014**, *75*, 11–18. [CrossRef]
66. de Lima Mesquita, A.; Barrero, N.G.; Fiorelli, J.; Christoforo, A.L.; De Faria, L.J.G.; Lahr, F.A.R. Eco-Particleboard Manufactured from Chemically Treated Fibrous Vascular Tissue of Acai (*Euterpe oleracea Mart.*) Fruit: A New Alternative for the Particleboard Industry with Its Potential Application in Civil Construction and Furniture. *Ind. Crops Prod.* **2018**, *112*, 644–651. [CrossRef]
67. Buratti, C.; Barbanera, M.; Lascaro, E.; Cotana, F. Optimization of Torrefaction Conditions of Coffee Industry Residues Using Desirability Function Approach. *Waste Manag.* **2018**, *73*, 523–534. [CrossRef]

68. Mati-Baouche, N.; De Baynast, H.; Michaud, P.; Dupont, T.; Leclaire, P. Sound Absorption Properties of a Sunflower Composite Made from Crushed Stem Particles and from Chitosan Bio-Binder. *Appl. Acoust.* **2016**, *111*, 179–187. [CrossRef]
69. Jiang, Y.; Lawrence, M.; Zhang, M.; Cui, J. Industrial Bio-Based Plant Aggregates as Hygric and Insulating Construction Materials for Energy Efficient Building. *Front. Chem. Sci. Eng.* **2020**, *16*, 1532. [CrossRef]
70. Arufe, S.; Hellouin de Menibus, A.; Leblanc, N.; Lenormand, H. Physico-Chemical Characterisation of Plant Particles with Potential to Produce Biobased Building Materials. *Ind. Crops Prod.* **2021**, *171*, 113901. [CrossRef]
71. Ahmad, M.R.; Chen, B.; Haque, M.A.; Saleem Kazmi, S.M.; Munir, M.J. Development of Plant-Concrete Composites Containing Pretreated Corn Stalk Bio-Aggregates and Different Type of Binders. *Cem. Concr. Compos.* **2021**, *121*, 104054. [CrossRef]
72. Mazhoud, B.; Collet, F.; Prétot, S.; Lanos, C. Effect of Hemp Content and Clay Stabilization on Hygric and Thermal Properties of Hemp-Clay Composites. *Constr. Build. Mater.* **2021**, *300*, 123878. [CrossRef]
73. Maskell, D.; Thomson, A.; Walker, P.; Lemke, M. Determination of Optimal Plaster Thickness for Moisture Buffering of Indoor Air. *Build. Environ.* **2018**, *130*, 143–150. [CrossRef]
74. Laborel-Préneron, A.; Magniont, C.; Aubert, J.-E. Characterization of Barley Straw, Hemp Shiv and Corn Cob as Resources for Bioaggregate Based Building Materials. *Waste Biomass Valoriz.* **2017**, *9*, 1095–1112. [CrossRef]
75. Benallel, A.; Tilioua, A.; Ettakni, M.; Ouakarrouch, M.; Garoum, M.; Ahmed Alaoui Hamdi, M. Design and Thermophysical Characterization of New Thermal Insulation Panels Based on Cardboard Waste and Vegetable Fibers. *Sustain. Energy Technol. Assess.* **2021**, *48*, 101639. [CrossRef]
76. Bertolini, M.S.; de Morais, C.A.G.; Christoforo, A.L.; Bertoli, S.R.; dos Santos, W.N.; Lahr, F.A.R. Acoustic Absorption and Thermal Insulation of Wood Panels: Influence of Porosity. *BioResources* **2019**, *14*, 3746–3757. [CrossRef]
77. Glé, P.; Gourdon, E.; Arnaud, L. Acoustical Properties of Materials Made of Vegetable Particles with Several Scales of Porosity. *Appl. Acoust.* **2011**, *72*, 249–259. [CrossRef]
78. Romano, A.; Bras, A.; Grammatikos, S.; Shaw, A.; Riley, M. Dynamic Behaviour of Bio-Based and Recycled Materials for Indoor Environmental Comfort. *Constr. Build. Mater.* **2019**, *211*, 730–743. [CrossRef]
79. Ratiarisoa, R.V.; Magniont, C.; Ginestet, S.; Oms, C.; Escadeillas, G. Assessment of Distilled Lavender Stalks as Bioaggregate for Building Materials: Hygrothermal Properties, Mechanical Performance and Chemical Interactions with Mineral Pozzolanic Binder. *Constr. Build. Mater.* **2016**, *124*, 801–815. [CrossRef]
80. Wolkoff, P. Indoor Air Humidity, Air Quality, and Health—An Overview. *Int. J. Hyg. Environ. Health* **2018**, *221*, 376–390. [CrossRef] [PubMed]
81. Verdier, T.; Coutand, M.; Bertron, A.; Roques, C. A Review of Indoor Microbial Growth across Building Materials and Sampling and Analysis Methods. *Build. Environ.* **2014**, *80*, 136–149. [CrossRef]
82. Johansson, P.; Mjörnell, K.; Arfvidsson, J. Examples of Characteristics of Wood That Affect Mould Growth: A Meta-Analysis. *Eur. J. Wood Wood Prod.* **2017**, *75*, 603–613. [CrossRef]
83. Gonçalves, F.G.; Paes, J.B.; Lopez, Y.M.; de Alcântara Segundinho, P.G.; de Oliveira, R.G.E.; Fassarella, M.V.; Brito, A.S.; Chaves, I.L.S.; Martins, R.S.F. Resistance of Particleboards Produced with Ligno-Cellulosic Agro-Industrial Wastes to Fungi and Termites. *Int. Biodeterior. Biodegrad.* **2021**, *157*, 105159. [CrossRef]
84. Stefanowski, B.K.; Curling, S.F.; Ormondroyd, G.A. A Rapid Screening Method to Determine the Susceptibility of Bio-Based Construction and Insulation Products to Mould Growth. *Int. Biodeterior. Biodegrad.* **2017**, *116*, 124–132. [CrossRef]
85. Brambilla, A.; Sangiorgio, A. Mould Growth in Energy Efficient Buildings: Causes, Health Implications and Strategies to Mitigate the Risk. *Renew. Sustain. Energy Rev.* **2020**, *132*, 110093. [CrossRef]
86. Johansson, P.; Svensson, T.; Ekstrand-Tobin, A. Validation of Critical Moisture Conditions for Mould Growth on Building Materials. *Build. Environ.* **2013**, *62*, 201–209. [CrossRef]
87. Johansson, P.; Ekstrand-Tobin, A.; Bok, G. An Innovative Test Method for Evaluating the Critical Moisture Level for Mould Growth on Building Materials. *Build. Environ.* **2014**, *81*, 404–409. [CrossRef]
88. Palumbo, M.; Lacasta, A.M.; Holcroft, N.; Shea, A.; Walker, P. Determination of Hygrothermal Parameters of Experimental and Commercial Bio-Based Insulation Materials. *Constr. Build. Mater.* **2016**, *124*, 269–275. [CrossRef]
89. Posani, M.; Veiga, R.; Freitas, V. Post-Insulating Traditional Massive Walls in Southern Europe: A Moderate Thermal Resistance Can Be More Effective than You Think. *Energy Build.* **2023**, *295*, 113299. [CrossRef]